A mathematical approach for optimizing telecentric digital holographic microscope design

Lei Jin[1,4], Aaron Au[1,4], Christopher M. Yip[1,2,3,4,*]

[1] Institute of Biomedical Engineering, 164 College St, University of Toronto, Toronto, ON, M5S 3G9, Canada

[2] Department of Chemical Engineering & Applied Chemistry, 200 College St, Toronto, ON, M5S 3E5, Canada

[3] Department of Biochemistry, University of Toronto, 1 King's College Circle, Toronto, ON M5S 1A8

[4] Donnelly Centre for Cellular & Biomolecular Research, University of Toronto, 160 College Street, Toronto, Ontario M5S 3E1, Canada

* christopher.yip@utoronto.ca

Abstract

Owing to its ability to rapidly acquire quantitative phase images (QPI), telecentric digital holographic microscopy (TDHM) has become an attractive tool for cell biology. However, as a computational imaging technique, it requires a well-aligned optical system in order to optimize the resolution of the resulting hologram. We report a mathematical model that describes the relationship between the optical configuration and the resulting components in the hologram, i.e. fringe size and Fourier spectrum. This model helps to simplify TDHM design by determining the optimal angle between the sample and reference beams based on the characteristics of the imaging sensor and illumination wavelengths.

Introduction

First introduced by Gabor to suppress the spherical aberration in electron microscopy, holography and its practical applications for amplitude and phase reconstruction of wavefronts emerged with the introduction of coherent illumination sources [1]. By adding a tilted reference wave in an approach known as off-axis holography, Leith and Upatnieks separated the conjugated wavefront (twin image) and reference intensity (zeroth-order) from the actual wavefront [2] to successfully reconstruct a 3D image from a hologram [3]. There has been keen interest in off-axis digital holographic microscopy (DHM) due to its ability to acquire quantitative phase information and infer the thickness and the refraction index of samples from a single exposure. These capabilities have been exploited in applications ranging from particle tracking [4], microelectromechanical systems characterization [5], to live-cell imaging [6].

Telecentric digital holographic microscopy (TDHM) improves on off-axis holographic microscopy by converting the spherical wavefront back to a planar wavefront at the camera sensor [7] [8]. This eliminates the need to compensate the parabolic phase aberration from the reconstructed complex field [9–11]. In holographic microscopy, image quality and resolution

are dependent on instrument parameters such as illumination wavelength, Fourier filter parameters, and beam tilt angle. For example, optimizing the angle between the object and reference beams allows for good separation of the +1 diffraction order resulting in higher spatial bandwidth [12], which translates to increased lateral resolution in the reconstructed images. The ability to estimate the sample phase is influenced by the contrast and density of the interference patterns in the hologram [13]. Accordingly, most TDHM systems make use of bulky and expensive rotation and piezo stages to make fine adjustments to the beam paths, which increases both the cost and size of the platforms[14]. To address this, we report a mathematical model that describes the relationship between the beam angle, illumination wavelength, and the resulting interference pattern seen in the hologram. This model eliminates the need for lengthy alignment procedures by calculating the optimal beam angle based on camera pixel size and illumination wavelength.

2. Method

For demonstrating the feasibility of this approach, a prototype TDHM was constructed. As seen in **Fig. 1**, the beam emitted by the laser (CUBE 640-40C, Coherent Inc.) is split (BS013, Thorlabs Inc.) into object and reference beams after passing through a beam expander (AC254-030-A-ML, AC254-060-A-ML, Thorlabs Inc.) fitted with a pinhole (P50K, Thorlabs Inc.). The reference beam is attenuated using a ND filter (NDC-50C-4M-A, Thorlabs Inc.) and enlarged 10x with a pair of lenses (AC254-030-A-ML, AC254-300-A-ML, Thorlabs Inc.) while the object beam passes through an objective (UPLanSApo, 20x/0.75, Olympus Inc.) and tube lens (AC508-180-A-ML, Thorlabs Inc.). The holographic interference pattern is generated when the reference and objective beans are redirected, using another beam splitter (BS031, Thorlabs Inc.), to intersect at the CMOS camera (BFS-U3-120S4M-CS, FLIR).

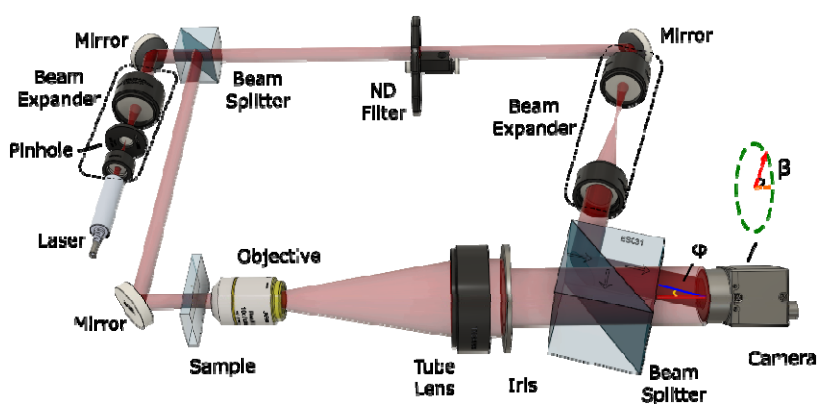

Fig 1. Schematic of TDHM prototype. φ represents the angle between the sample and reference beams, and β represents the rotation angle of the camera relative to the optical axis.

In TDHM, separation between the first-order and the zero-order is achieved by tilting the reference beam with respect to the object beam [9], as seen in **Figure 2 (d)**. The desired phase information is encoded in the first-order. A bandpass Fourier filter centered around the first-order peak is used to generate a phase image. It is important to optimize the position of the first-order peak and the size of the resulting filter mask as this impacts the spatial bandwidth of the result image. Determining the optimal beam angle is essential to maximize image quality as it impacts the location of the first-order peak in Fourier space.

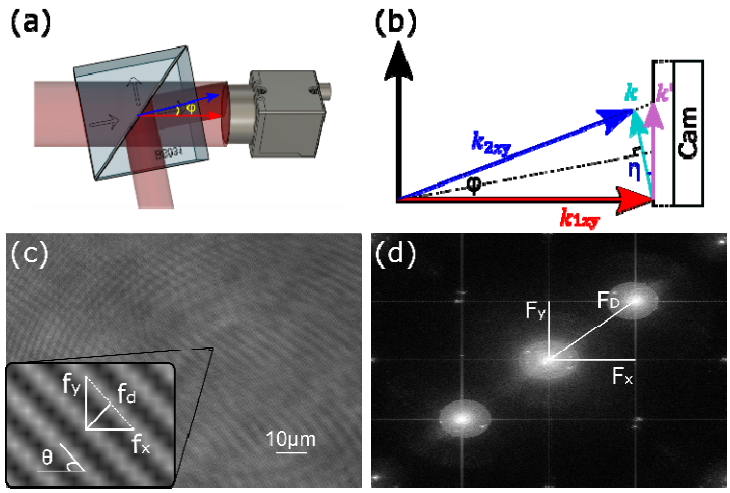

Fig 2. Interference resulting from the difference in beam angles. Two beams meet at the cube and then interfere at the camera sensor. The phase component can be described by wave vector **k**. The projection of the resulting interference wave vector **k'** should be very close to **k** since the residual angle η is close to 0° due to the small beam angle (<10°). The hologram (c) is obtained directly from the digital camera and (d) is the resulting Fourier spectrum, where f_x, f_y and f_d represent the interference fringe sizes, and F_x, F_y, F_D represents the corresponding first-order position in the Fourier spectrum. θ represents the fringe angle.

To characterize the relationship between beam angle and the position of the first order, we first determined how interference patterns on a camera sensor affect the position of first-order peaks in Fourier space. With a simple geometric relationship, as seen in **Fig. 2**, the distance between the interference fringes is described by [15]:

1

2

3

Where p_i is the pixel size of the camera and Δp_i is its sensor size in x and y. According to the geometric layout (**FIG.2 (a)** and **(b)**), the fringe size (f_d) and inclination (θ) are described by the position of the first order in the spectrum (**Eq.2** and **Eq.3**).

Assuming the optic wave of the DHM is propagating in a dielectric medium whose magnetic and electric permittivities are constant throughout the region of propagation and independent of the direction of the polarization, the effect of the medium can be neglected when we only consider the image intensity contrast on the camera sensor. The interference between the object and the reference beam can be represented by:

$$I_0 = {E_1}^2 + {E_2}^2 + 2\overrightarrow{E_1}\overrightarrow{E_2}\cos(\delta_2 - \delta_1)\#(4)$$

$$\delta_2 - \delta_1 = \left(\overrightarrow{k_2}\overrightarrow{r_2} - \overrightarrow{k_1}\overrightarrow{r_1}\right) - (\omega_2 - \omega_1)t + (\gamma_2 - \gamma_1)\#(5)$$

Where E_i is the amplitude of the two beams, $\vec{k}$ is wave-vector, ω represents the wave frequency, γ represents their initial phase, and δ represents their phase.

In this case, as the two beams are emitted by the same laser source, (ω_2-ω_1) and (γ_2- γ_1) are both equal to zero. Using ND filters and polarizers, the intensity of beams can be equalized (E_1=E_2=E_0). Assuming the object and reference arm are in the same plane (x-y plane), the interference expression can be simplified as:

$$I_0 = 2{E_0}^2 + 2{E_0}^2\cos\left(x\left(\overrightarrow{k_{2xy}} - \overrightarrow{k_{1xy}}\right)\right)\#(6)$$

Where $\overrightarrow{k_{1xy}}$ and $\overrightarrow{k_{2xy}}$ are wave vectors of the object and reference beam in the x-y plane, respectively.

Here, **Eq.6** represents the intensity distribution of the optic field encompassed by the two beams. The interference fringes are encoded in the phase difference of the two beam (k_{2xy}-k_{1xy}), As seen in **Fig. 2 (a)**, we assume these two beams converge at the center of the cube and then interfere at the camera sensor. In this case, we can describe the phase difference in **Eq. 6** by:

$$\overrightarrow{k_{2xy}} - \overrightarrow{k_{1xy}} = \mathrm{k}\cdot\sin\left(\frac{\varphi}{2}\right)\#(7)$$

From **Fig. 2 (b)**, we know that there is an error between k vector and the actual k' vector due to the residual angle η ($\varphi/2$ in this case). This error can be ignored when the camera is close enough to the front cube since the beam angle (φ) is generally small (<10°). With this

assumption, the interference pattern (**Eq. 6**) can be simplified as follows:

$$I_0 = 4{E_0}^2 \cdot cos^2\left(\mathrm{x} \cdot \mathrm{k} \cdot \sin\left(\frac{\varphi}{2}\right)\right) \#(8)$$

The distance between interference fringes f_d is exactly the period of this projected intensity distribution (**Eq.8**). The wave vector k can be described by $\left|\overrightarrow{k_1}\right| = \left|\overrightarrow{k_2}\right| = \frac{2\pi}{\lambda} = k$, where λ represents the laser wavelength. Thus, the fringe size is described as:

$$f_d = \frac{\lambda}{2sin\left(\frac{\varphi}{2}\right)} \#(9)$$

Combined with **Eq. 2**, the beam angle can be described as:

$$beam\ angle = \varphi = 2\arcsin\left(\frac{\lambda}{2f_d}\right)$$
$$= 2\arcsin\left(\frac{\lambda}{2} \cdot \sqrt{\left(\frac{F_x}{\Delta p_x \cdot p_x}\right)^2 + \left(\frac{F_y}{\Delta p_y \cdot p_y}\right)^2}\right) \#(10)$$

According to **Eq. 10**, the fringe size of the interference pattern is only dependent on the illumination wavelength and the beam angle. Furthermore, the position of the first-order peak in the Fourier spectrum is determined by the fringe size and its angle, as can be seen in **Eq. 3**. Accordingly, these two equations can be used to model the relationship between the beam angle and the corresponding interference pattern as well as the resulting Fourier spectrum.

3. Experiments

In order to verify this mathematical model, we performed three experiments on our TDHM prototype. According to **Eq. 10**, no change in fringe size is expected with respect to the position of the camera along the optical axis. We expect to see an inverse relationship between beam angle and fringe size, which can be verified via the experiment presented in **Fig. 3**. For our specific experimental setup, we know the mean squared error of this method is less than 0.131 μm^2.

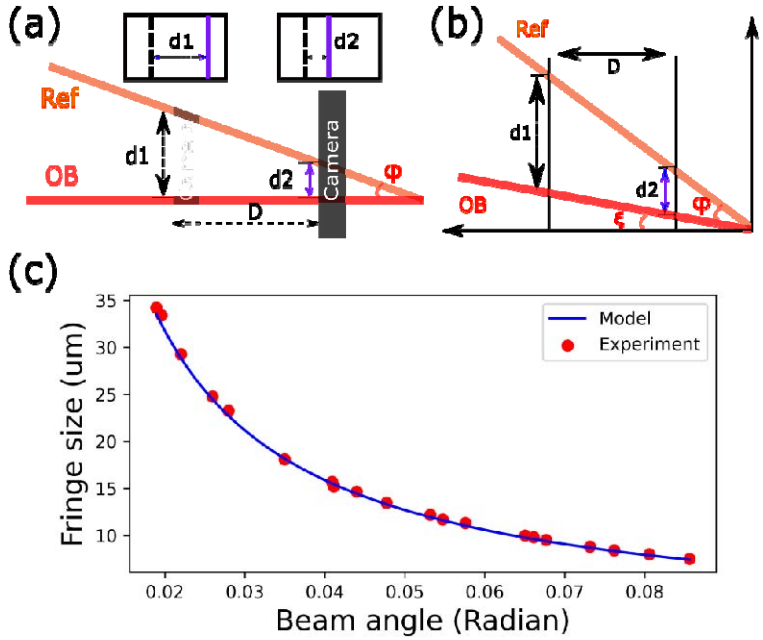

Fig 3. Experiment setting for beam angle: (a) Experimental set up, (b) error analysis and (c) result. Setting a line pattern into the object (black dotted) and reference arms (purple solid), respectively. The projected line distances and can be obtained by moving the camera at a distance D along the optical axis.

In order to determine the incoming beam angle, a line pattern orthogonal to the rotational axis was introduced into the beam paths, as seen in **Supplementary Fig. 1**. Since the beams are collimated, the projection of the line pattern is the same at any point along the path, and only the distance between the reference (Ref) and object (OB) beams changes **Fig. 3 (a)**. The beam angle (φ) can be determined by measuring the distances of the lines at two different positions along the optical axis. It was characterized using a simple geometric relationship:

Where and are the distances between the projected lines, and D is the displacement of the camera.

However, we must account for a small angle (ξ) between the OB path and the optical axis to compensate for misalignment, as seen in **Figure 3 (B)**. Accordingly, when the beam angle φ is between 0° and ~ 10°, it can be described as:

If properly aligned, the residual angle is typically less than 0.3°, and the approximation can be simplified to:

We note that the simplified **Eq. 13** is the same as **Eq. 11** as we assumed that the residual angle is negligible. The fringe size for each trial was translated into the Fourier spectrum by **Eq. 2**. The calculated data from the experiment was compared to the model, **Eq. 10**. The above calculations assume that the object and reference beams interfere in the same plane as the pixel grid (x or y direction). Thus, the direction of the fringes and corresponding first order would be orthogonal to the field of view, i.e. vertically or horizontally. However, as shown in Daniel's work [16], the optimal first-order position should be located on the diagonal of the Fourier spectrum, which is usually achieved by tilting the reference beam until the angle of the fringes is optimized. A simpler approach would be to rotate the camera around the optical axis to change the location of the first-order peak in the Fourier spectrum, as demonstrated in **Figure 4 (a)**.

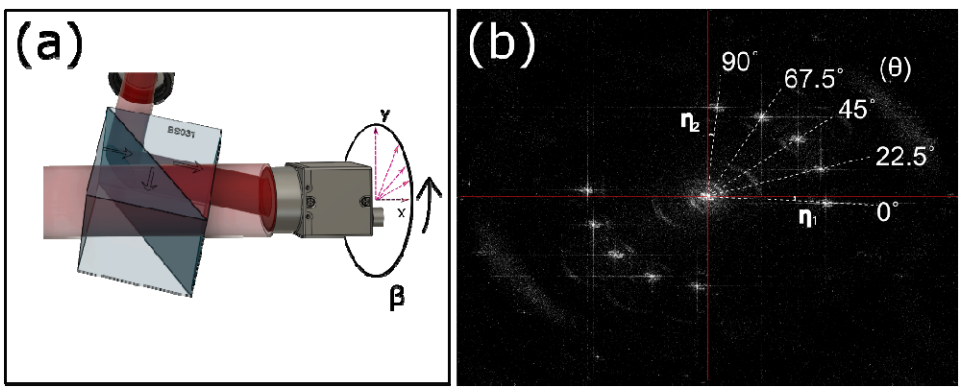

Fig 4. Optimization of camera rotation: (a) Schematic of the experiment where the camera is rotated along the optical axis, (b) Combined Fourier spectrum of different camera rotation angles, where η_1 and η_2 are typical system errors mainly from the residual beam angles that are calculated as 0.2˚ ± 0.03˚.

The position of the first order, specifically the angle at which the first order rotates around, is correlated to the camera rotation angle as described in **Eq. 3**. In our prototype, the pixel size of the camera (BFS-U3-120S4M-CS, FLIR) is 1.85 μm (=1.85μm) and the sensor size is 4000 x 3000 ( ). From **Eq. 3**, we would therefore expect to see the following relationship,

Where θ represents the fringe direction.

Eq.14 was verified by rotating the camera around the optical axis to 5 different angles (θ), 0˚, 22.5˚, 45˚, 67.5˚ and 90˚, as seen in **Figure. 4**. There exist some rotational errors in the first order (η_1 and η_2) of the spectrum when setting the camera to 0˚ and 90˚, which arise due to the fact that the beams do not perfectly interfere at the same plane and the object beam was not perfectly parallel to the optical axis. From our model, the corresponding residual beam angle (0.2˚ ± 0.03˚) can be easily obtained from **Eq. 10**. This error can be easily compensated for by further rotating the camera. The error of the beam angle is negligible, < 1°. Moreover, as seen in Daniel's work [16], the optimal first-order position was located on the diagonal of the Fourier spectrum when the camera was rotated to 45˚, regardless of sensor shape.

For TDHM, another consideration is fringe contrast in which the continuous fringe patterns are integrated and converted into discretized 2D arrays as the holograms are acquired using a pixel-wise sensor. If the frequency of the fringe pattern is too small, the contrast of the fringe patterns would be reduced as more of the wave pattern would be integrated over a single pixel. It is crucial to get good contrast with the fringe pattern as it holds the phase information. The fringe contrast can be evaluated from the full width at half maximum of the first-order peak in the corresponding Fourier spectrum. We expect to resolve a star-like first order with long tails when the fringe contrast is sufficient. To achieve this, and to satisfy Nyquist criteria, we need to carefully design the fringe size to be an integer multiple at least twice that of the camera pixel size **Supplementary Fig.2**.

Given the above constraints, the last factor to consider is the optimum integer multiple for the camera pixel size. A small fringe size could result in a weak contrast but a larger fringe size would decrease the final resolution, **Figure 5**. According to Emilio's work [12], the radius of the FFT filter should be 1/3 of the distance between the zero order and first order peak, allowing one to calculate the radius of the FFT filter. Given this criterion and the goal of selecting a fringe size that was an integer multiple of the camera's pixel size, a fringe size 3x that of the pixel size (5.55 μm, resulting in a beam angle of 6.6˚) was selected. **Figure 5 (cam1: 6.6°)**.

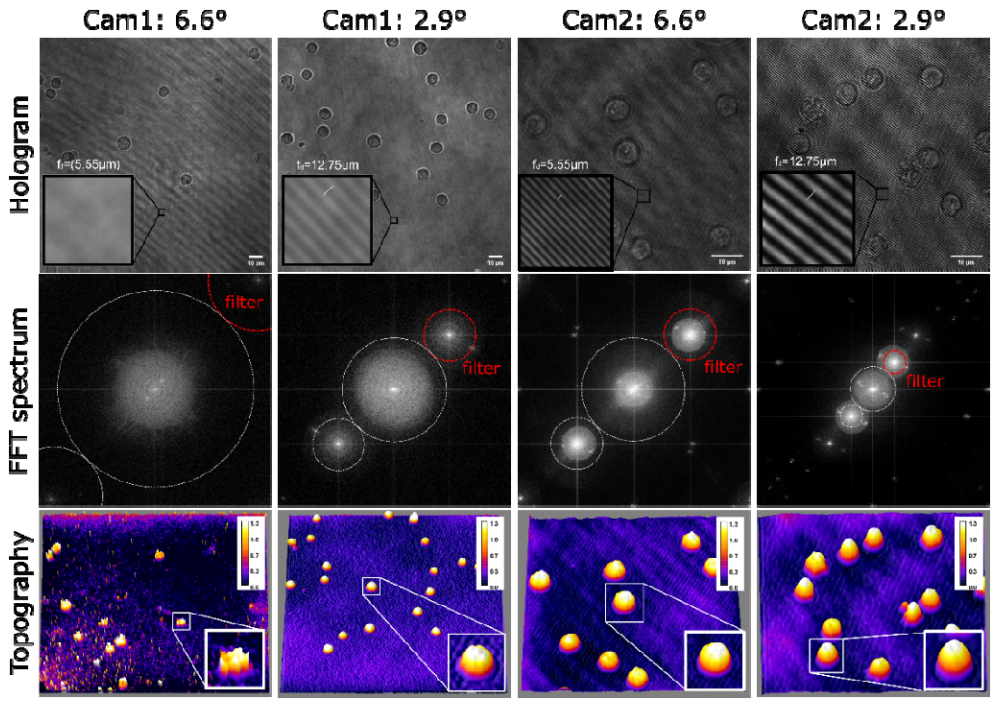

Fig 5. TDHM result of HeLa cells with different beam angles and camera pixel sizes. Cam 1 is Iris 15, Teledyne Photometrics Inc (pixel size: 4.25μm); Cam 2 is BFS-U3-120S4M-CS, FLIR Inc (pixel size: 1.85μm). The fringe size achieves 3 times pixel size for two cameras when the beam angle is set as 2.9°(Cam 1) and 6.6° (Cam 2), respectively. The illumination wavelength is 640nm.

Selection and application of an appropriate FFT filter is an essential step in TDHM pipeline. To achieve high lateral resolution, the FFT filter mask needs to be large enough to conclude complete high-frequency components of the hologram but avoid any intensity information in zero order. Therefore, the parameters of pixel size and wavelength need to be considered, as shown in **Figure 5,** while the objective needs to fulfill **Eq. 15** in order to obtain the diffraction-limit lateral resolution.

Where *NA* and *Mag* are the numerical aperture and the magnification of the optical objectives, respectively, the λ is the wavelength of the illumination, and the *Pixel* is the pixel size of the digital camera.

4. Conclusion

This paper derives a mathematical model describing the relationship between beam angle, fringe pattern, illumination wavelength and the corresponding Fourier spectrum of a hologram. When given the wavelength of the laser and the camera pixel size, the model could

be employed to estimate the optimal beam angle and related fringe size. This model provides a theory to guide and optimize the design of a TDHM. While experimental validation confirmed an average squared error is $0.131\mu m^2$, we have further proposed rotating the digital camera instead of adjusting the spatial beam angle to simplify alignment.

This model was based on the assumption that two beams first meet at the center of the cube and propagate in a dielectric homogenous medium. If they meet and interfere at the camera sensor directly, the interference wave vector k (**Eq. 7**) needs to be recalculated to re-correct this model. We also note that no matter the size or shape of the camera, the optimal camera rotation angle should always be equal to 45° for square pixel cameras. Furthermore, the fringe size should be at least double the camera pixel size and diffraction-limited lateral resolution will be achieved by selecting an objective that meets the criteria described in **Eq.15**

The proposed model could be applied to more complicated off-axis DHM configurations such as multiwavelength and multi-angle DHM since the relationship between the beam angle and the corresponding Fourier spectrum can be easily calculated. Multiwavelength DHM was introduced to eliminate the 2π phase ambiguity (phase discontinuity) and extend the axial measurement range [17]. In such a system, a second set of beams creates extra first orders in the Fourier spectrum, requiring extensive alignment [18], which is time-consuming. The recently described multi-angle DHM platform also shares the same consideration due to its complex configuration [19] [20]. The presented model addresses all these concerns in a straightforward and experimentally tractable approach.

Funding. We thank Huawei Canada for providing financial support for this project under their Research Program Agreement program with the University of Toronto: Project number: 505967

Acknowledgement. We thank Huawei Canada for providing financial support for this project under their Research Program Agreement program with the University of Toronto. Thanks to members of Professor Aaron Wheeler's group at the University of Toronto for providing the HeLa cells used in this study.

Disclosures. The authors declare no conflicts of interest.

Data availability. Data underlying the results resented in this paper are not publicly available at this time but may be obtained from the authors upon reasonable request.

REFERENCES

1. T. H. Maiman, (University of Chicago Press, 2010), pp. 113–114.

2. E. N. Leith and J. Upatnieks, J. Opt. Soc. Am. **52**, 1123 (1962).
3. E. N. Leith and J. Upatnieks, J. Opt. Soc. Am. **54**, 1295 (1964).
4. P. Memmolo, L. Miccio, M. Paturzo, G. D. Caprio, G. Coppola, P. A. Netti, and P. Ferraro, Adv. Opt. Photon., AOP **7**, 713 (2015).
5. G. Coppola, P. Ferraro, M. Iodice, S. D. Nicola, A. Finizio, and S. Grilli, Meas. Sci. Technol. **15**, 529 (2004).
6. B. Kemper, D. D. Carl, J. Schnekenburger, I. Bredebusch, M. Schäfer, W. Domschke, and G. von Bally, JBO **11**, 034005 (2006).
7. A. I. Doblas, E. Sánchez-Ortiga, M. Martínez-Corral, G. Saavedra, and J. Garcia-Sucerquia, JBO **19**, 046022 (2014).
8. E. Sánchez-Ortiga, P. Ferraro, M. Martínez-Corral, G. Saavedra, and A. Doblas, J. Opt. Soc. Am. A, JOSAA **28**, 1410 (2011).
9. M. K. Kim, SR **1**, 018005 (2010).
10. B. Kemper and G. von Bally, Appl. Opt., AO **47**, A52 (2008).
11. T. Kreis, (John Wiley & Sons, 2006).
12. E. Sánchez-Ortiga, A. Doblas, G. Saavedra, M. Martínez-Corral, and J. Garcia-Sucerquia, Appl. Opt., AO **53**, 2058 (2014).
13. M. Liebling, "On Fresnelets, interference fringes, and digital holography," https://infoscience.epfl.ch/record/33450.
14. M. K. Kim, L. Yu, and C. J. Mann, J. Opt. A: Pure Appl. Opt. **8**, S518 (2006).
15. J. W. Goodman, Publishers, Englewood, Colorado (2005).
16. D. Carl, B. Kemper, G. Wernicke, and G. von Bally, Appl. Opt., AO **43**, 6536 (2004).
17. J. Gass, A. Dakoff, and M. K. Kim, Opt. Lett., OL **28**, 1141 (2003).
18. J. Kühn, T. Colomb, F. Montfort, F. Charrière, Y. Emery, E. Cuche, P. Marquet, and C. Depeursinge, Opt. Express, OE **15**, 7231 (2007).
19. J. Lu, Y. Zeng, X. Chang, Y. Hong, and X. Hu, Journal of Vacuum Science & Technology B **38**, 064003 (2020).
20. J. Dong, C. Jiang, and S. Jia, Opt. Lett., OL **41**, 4301 (2016).

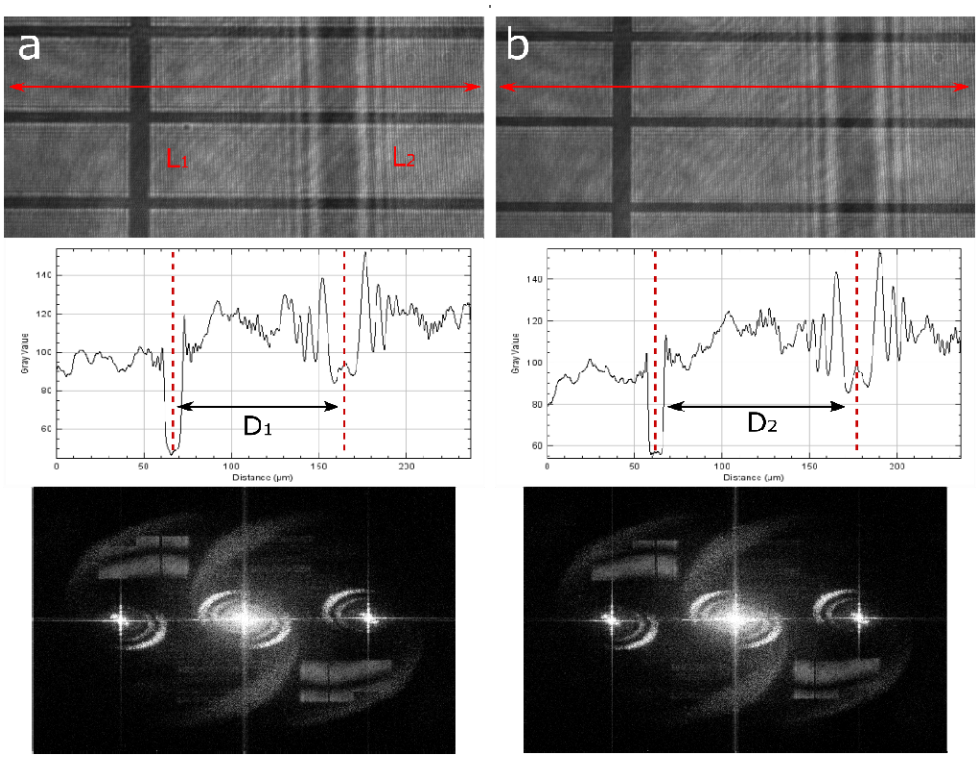

Fig. S1. Scaling of the line samples: (a) and (a) are the results of line samples in 5 mm displacement of the camera, separately. After Gaussian blurring the raw hologram, the line distance can be detected in their line plot. We can notice that, with the displacement of the camera, the line distance changed, but their Fourier spectrum was the same. It means the camera displacement does not impact the fringe size.

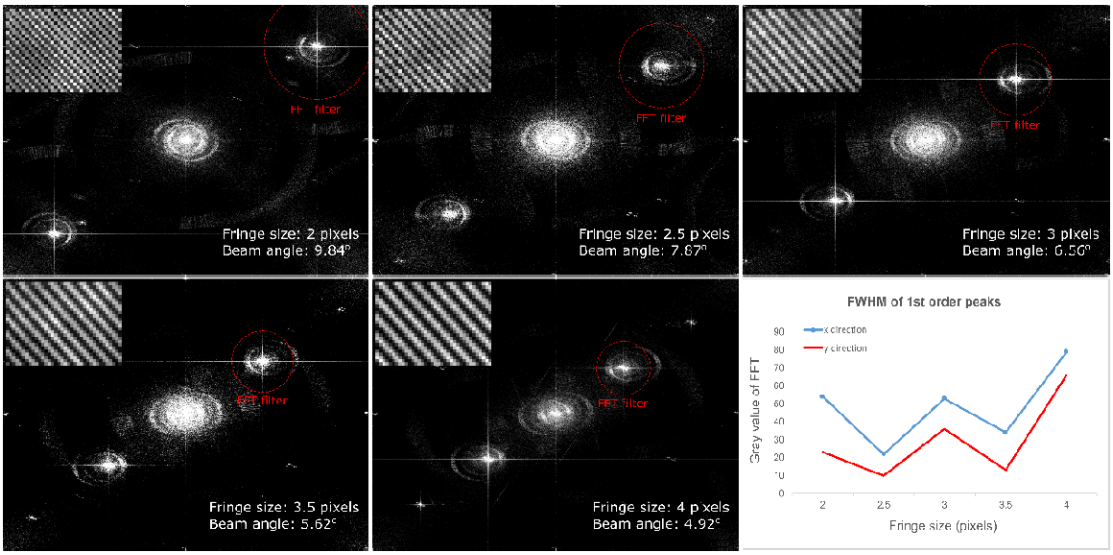

Fig. S2 Optimization of the fringe size: The camera is rotated 45˚ around the optical axis but with variable beam angles. It is noticeable that the contrast of the fringe alters with different beam angles. This figure shows the cropped holograms with their Fourier spectrum. According to their gray value plot of the corresponding first-order full width at half maximum (FWHM), we conclude that the fringe size should be integer than the camera pixel size. Considering the FFT filter, we suggest 3 times the pixel size.